A Comprehensive Exploration of Na$^+$ Ion Transport in NaSICONs Using Molecular Dynamics Simulations

Supporting Information

Judith Schuett,[a,b] Steffen Neitzel-Grieshammer[a*], Shuta Takimoto[c], Ryo Kobayashi[d], Masanobu Nakayama[c]

[a] Faculty of Chemical Engineering, FH Münster – University of Applied Sciences, Stegerwaldstraße 39, 48565 Steinfurt, Germany.

[b] Institute of Physical Chemistry, RWTH Aachen University, Landoltweg 2, 52056 Aachen, Germany.

[c] Department of Advanced Ceramics, Nagoya Institute of Technology, Gokiso, Showa, Nagoya 466-8555, Japan.

[d] Department of Applied Physics, Nagoya Institute of Technology, Gokiso, Showa, Nagoya 466-8555, Japan.

*steffen.neitzel-grieshammer@fh-muenster.de

1. Impact on Thermostat on Ionic Diffusion

To evaluate the influence of the thermostat on ionic diffusion, additional FFMD simulations were conducted under the NVE ensemble, omitting the heat bath. These simulations show that the diffusion coefficients increase by approximately a factor of 1.4 on average (Fig. S1). Nevertheless, the overall trend of concentration-dependent diffusion behavior remains largely unchanged.

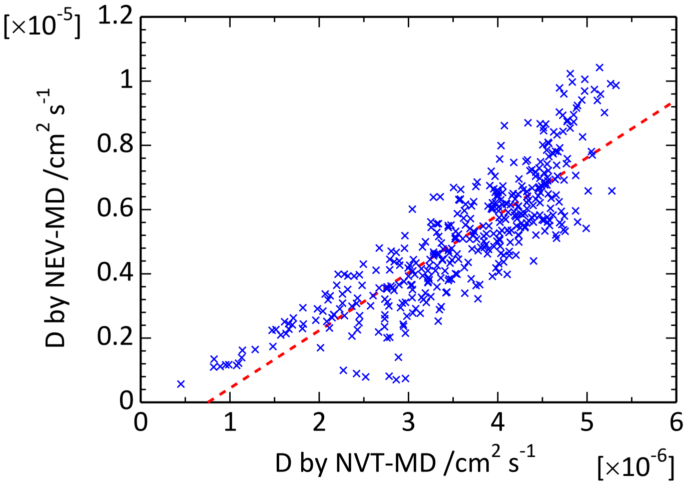

Figure S1. Comparison of diffusion coefficient of Na$^+$ ions in $Na_{1+x+y}Sc_yZr_{2-y}Si_xP_{3-x}O_{12}$ ($0 \le x \le 3$; $0 \le y \le 2$) at 598 K, obtained by NVT-MD simulations with the Langevin thermostat (horizontal axis) and NEV-MD simulations without a heat bath (vertical axis). The red line represents the linear regression fit, with a coefficient of determination (R^2) of 0.72.

2. Optimization of FF Parameters

The force field (FF) parameters are optimized using the Cuckoo Search (CS) algorithm. The metaheuristic optimization is evaluated by the loss function L^1 assessing the difference for the radial distribution function (RDF) $g(r)$, angular distribution function (ADF) $h(\theta)$, and equilibrium volume (V_0) obtained by FF molecular dynamics (FFMD) and by ab-initio molecular dynamics (AIMD) simulations.

$$L = L_{\mathrm{RDF}} + L_{\mathrm{ADF}} + L_{\mathrm{V}} \tag{S1}$$

$$L_{\mathrm{RDF}} = \frac{1}{N_p}\sum_{p}^{N_p}\left(\frac{\sum_{i=1}^{N_{\mathrm{RDF}}}\left(g_{\mathrm{FF}}(r_i) - g_{\mathrm{AI}}(r_i)\right)^2}{\sum_{i=1}^{N_{\mathrm{RDF}}} g_{\mathrm{AI}}(r_i)^2}\right) \tag{S2}$$

$$L_{\mathrm{ADF}} = \frac{1}{N_t}\sum_{t}^{N_t}\left(\frac{\sum_{i=1}^{N_{\mathrm{ADF}}}\left(h_{t,\mathrm{FF}}(\theta_i) - h_{t,\mathrm{AI}}(\theta_i)\right)^2}{\sum_{i=1}^{N_{\mathrm{ADF}}} h_{t,\mathrm{AI}}(\theta_i)^2}\right) \tag{S3}$$

$$L_{\mathrm{V}} = \frac{(V_{\mathrm{FF}} - V_{\mathrm{AI}})^2}{{V_{\mathrm{AI}}}^2} \tag{S4}$$

with N_p and N_t being the number of pairs p and triplets t considered, respectively. N_{RDF} (here: N_{RDF} = 100) and N_{ADF} (here: N_{ADF} = 180) is the number of sampling points in the RDFs and ADFs, respectively.

The determination of the FF parameters of the six-component NaSICON structure $Na_{1+x+y}Sc_yZr_{2-y}Si_xP_{3-x}O_{12}$ is challenging due to the large number of parameters to be optimized. Thus, the CS optimization is performed in several steps: (i) Optimization of the FF parameters in the co-substituted training system $Na_3ScZrSiP_2O_{12}$, which serves as a preliminary assessment to gauge the accuracy of the obtained FF parameters; (ii) Optimization in the single-substituted training system $Na_3Zr_2Si_2PO_{12}$; (iii) Final optimization in the co-substituted training system $Na_3ScZrSiP_2O_{12}$ using previously obtained FF parameters as initial guess. Each step is discussed in detail in the following to describe the overall optimization process.

Step (i): Fig. S2 shows the evolution of the loss function (Eq. S1) during the FF optimization in the co-substituted $Na_3ScZrSiP_2O_{12}$ training system. As the number of CS generations increases, the loss function value decreases. Convergence is achieved within 1400 CS generations, as indicated by the low loss function value of L = 5.38·10^{-3}. The obtained FF parameters are given in Table S1.

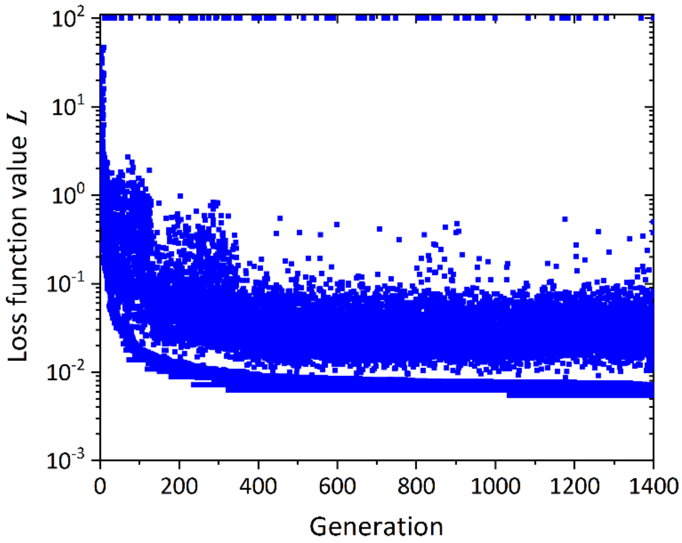

Figure S2. Evolution of the loss function L during the (i) CS optimization in the co-substituted $Na_3ScZrSiP_2O_{12}$ training system.

Table S1. FF parameters derived from the (i) CS optimization in the $Na_3ScZrSiP_2O_{12}$ training system. $D_{0,XO}$ is the equilibrium well depth, $r_{0,XO}$ is the equilibrium bond distance between species *X* and O^{2-}, and α_{XO} is the width of the Morse potential. r_X is the effective ionic radius of species *X* of the Coulomb potential. λ_{OXO} is the equilibrium well depth and $\gamma_{0,OXO}$ is the equilibrium angle between O^{2-}-*X*-O^{2-} of the Stillinger Weber potential. *X* represents the cationic species and O is O^{2-} ions.

Species	$D_{0,XO}$ (eV)	$r_{0,XO}$ (Å)	α_{XO} (Å^{-1})	r_X, r_O (Å)	$\lambda_{0,OXO}$ (eV)	$\gamma_{0,OXO}$ ()
Na^+	0.66	2.09	1.85	1.01	—	—
Sc^{3+}	2.26	1.81	1.89	1.06	0.85	0.21
Zr^{4+}	2.45	1.77	1.72	1.03	0.68	−0.12
Si^{4+}	4.90	1.57	2.55	0.85	1.34	−0.52
P^{5+}	3.61	1.41	2.76	0.63	0.92	−0.40
O^{2-}	—	—	—	0.80	—	—

Using the obtained FF parameters, FFMD simulations are conducted not only in the co-substituted training system $Na_3ScZrSiP_2O_{12}$ but also in the single-substituted target systems $Na_3Zr_2Si_2PO_{12}$ and $Na_2ScZrP_3O_{12}$. Fig. S3 compares the obtained RDFs of the cation-O^{2-} pairs and ADFs of the of O^{2-}-cation-O^{2-} triplets of the structural framework with the results from previous AIMD simulations. This comparison is used to evaluate the accuracy of the FF parameters in reproducing the NaSICON structure. The FF parameters reproduce well the AIMD results of the Sc^{3+}-O^{2-} and Zr^{4+}-O^{2-} pairs as well as the angles of the triplets in $Na_3ScZrSiP_2O_{12}$. But the RDFs of the Si^{4+}-O^{2-} and P^{5+}-O^{2-} pairs at about 4 Å in $Na_3ScZrSiP_2O_{12}$ (Fig. S3a), the RDFs of the ion pairs at distances $r > 3.5$ Å in $Na_3Zr_2Si_2P_1O_{12}$ (Fig. S3c) and the RDF of the P^{5+}-O^{2-} pairs at about 4 Å in $Na_2Sc_1Zr_1P_3O_{12}$ (Fig. S3e) are not accurately described. It seems to be more difficult to obtain accurate FF parameters of the Si^{4+}-O^{2-} and P^{5+}-O^{2-} interactions, probably due to the different radii of the Si^{4+}- and P^{5+}-cations occupying the same lattice site ($r_{Si^{4+}}$ = 0.26 Å, $r_{P^{5+}}$ = 0.17 Å), in contrast to the Sc^{3+}-O^{2-} and Zr^{4+}-O^{2-} interactions, where the radii of Sc^{3+}- and Zr^{4+}-cations are similar ($r_{Sc^{3+}}$ = 0.74 Å, $r_{Zr^{4+}}$ = 0.72 Å).[2]

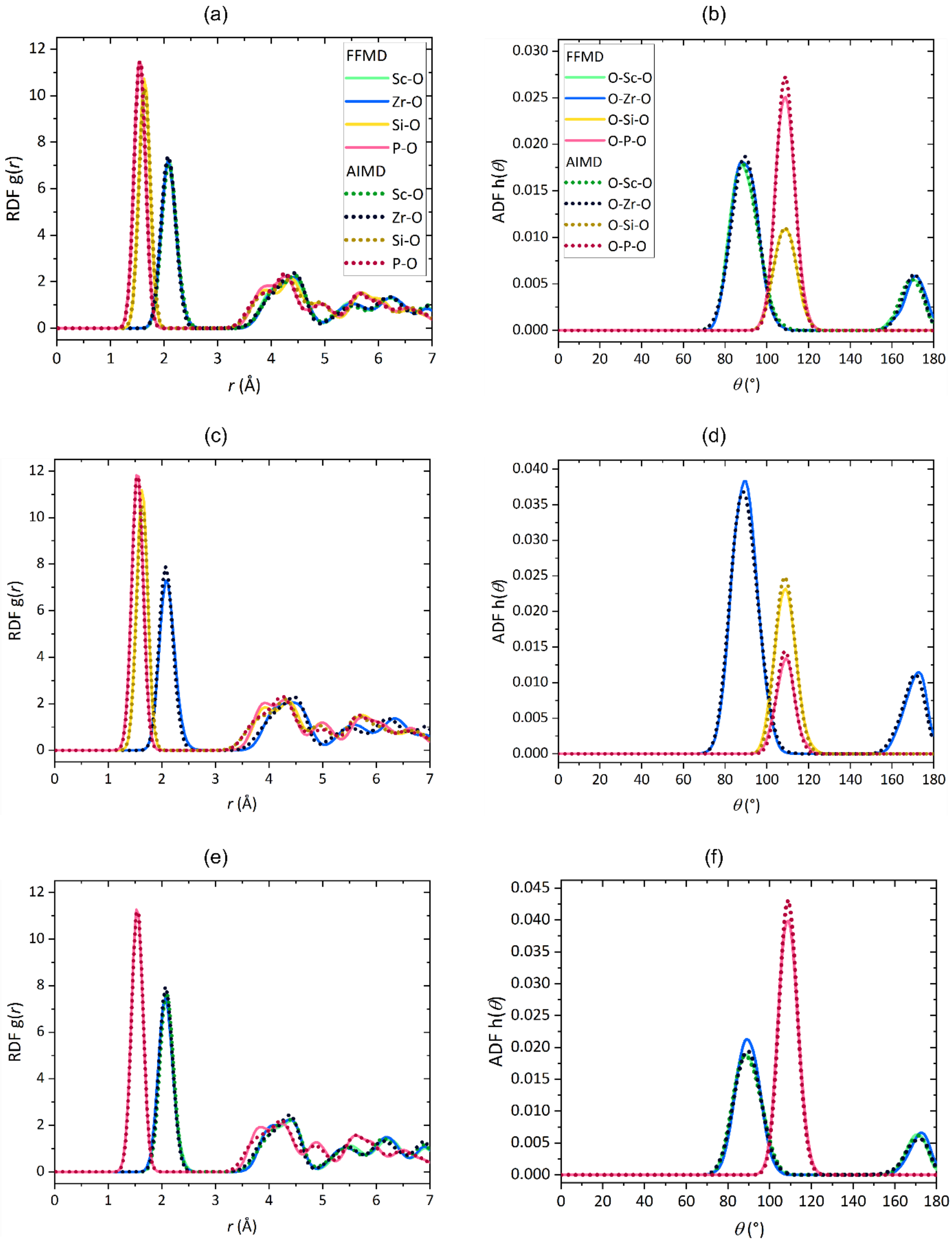

Figure S3. (a, c, e) RDFs of cation-O^{2-} pairs and (b, d, f) ADFs of O^{2-}-cation-O^{2-} triplets of the structural framework of (a, b) $Na_3ScZrSiP_2O_{12}$, (c, d) $Na_3Zr_2Si_2PO_{12}$, and (e, f) $Na_2ScZrP_3O_{12}$. The distribution functions obtained by FFMD with FF parameters derived from the (i) CS optimization are shown as solid lines and those obtained by AIMD are shown as dashed lines.

Moreover, FFMD simulations of $Na_{1+x}Zr_2Si_xP_{3-x}O_{12}$ ($0 \leq x \leq 3$) are performed at 598 K using the optimized FF parameters. Fig. S4 compares the resulting conductivities with literature data obtained from experiments[3–6] and KMC simulations at 573 K.[7,8] The obtained conductivities do not align with literature data. The discrepancies indicate that the interactions between the migrating Na^+ ions and the framework ions are not adequately captured by the FF parameters. However, the Na^+-cation interactions are crucial for the Na^+ transport in NaSICONs, as described in our previous study.[9,8]

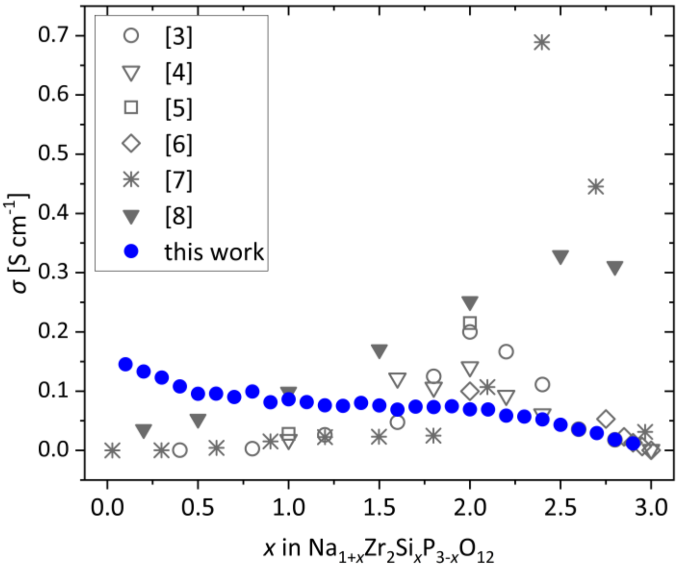

Figure S4. Comparison of Na^+ ion conductivity of $Na_{1+x}Zr_2Si_xP_{3-x}O_{12}$ ($0 \leq x \leq 3$) obtained by FFMD simulations at 598 K using FF parameters derived from the (i) CS optimization (blue) with data from experimental studies[3–6] and KMC simulations[7,8] at 573 K.

Step (ii): The direct determination of adequate FF parameters of the six-component NaSICON structure is not challenging due to the large number of parameters involved. Therefore, a pre-optimization step is performed using a five-component NaSICON training system. Fig S5 depicts the evolution of the loss function during the FF optimization in the single-substituted training system $Na_3Zr_2Si_2P_1O_{12}$. Convergence is achieved within 1000 CS generations ($L = 3.32 \cdot 10^{-3}$). The obtained FF parameters are listed in Table S2.

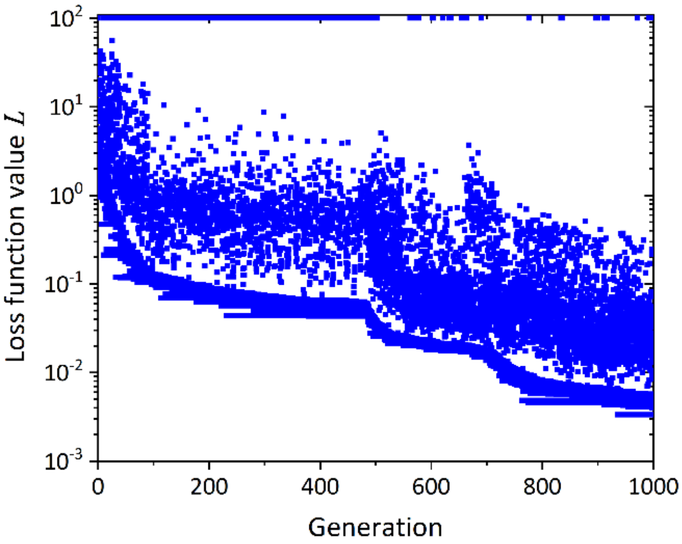

Figure S5. Evolution of the loss function L during the (ii) CS optimization in the single-substituted training system $Na_3Zr_2Si_2PO_{12}$.

Table S2. FF parameters derived from the (ii) CS optimization in the $Na_3Zr_2Si_2PO_{12}$ training system. $D_{0,XO}$ is the equilibrium well depth, $r_{0,XO}$ is the equilibrium bond distance between species *X* and O^{2-}, and α_{XO} is the width of the Morse potential. r_X is the effective ionic radius of species *X* of the Coulomb potential. λ_{OXO} is the equilibrium well depth and $\gamma_{0,OXO}$ is the equilibrium angle between O^{2-}-*X*-O^{2-} of the Stillinger Weber potential. *X* represents the cationic species and O the O^{2-} ions.

Species	$D_{0,XO}$ (eV)	$r_{0,XO}$ (Å)	α_{XO} (Å^{-1})	r_X, r_O (Å)	$\lambda_{0,OXO}$ (eV)	$\gamma_{0,OXO}$ ()
Na^+	0.48	2.17	1.94	1.05	—	—
Zr^{4+}	2.99	1.86	1.70	0.70	1.21	-0.033
Si^{4+}	2.96	1.56	3.18	0.60	1.51	0.17
P^{5+}	5.62	1.42	2.33	0.88	0.91	0.68
O^{2-}	—	—	—	0.85	—	—

As shown in Fig. S6, the RDFs of cation-O^{2-} pairs and ADFs of O^{2-}-cation-O^{2-} triplets of the structural framework of $Na_3Zr_2Si_2PO_{12}$ obtained from FFMD simulations using the optimized FF parameters agree well with the results of previous AIMD simulations, validating the successful optimization.

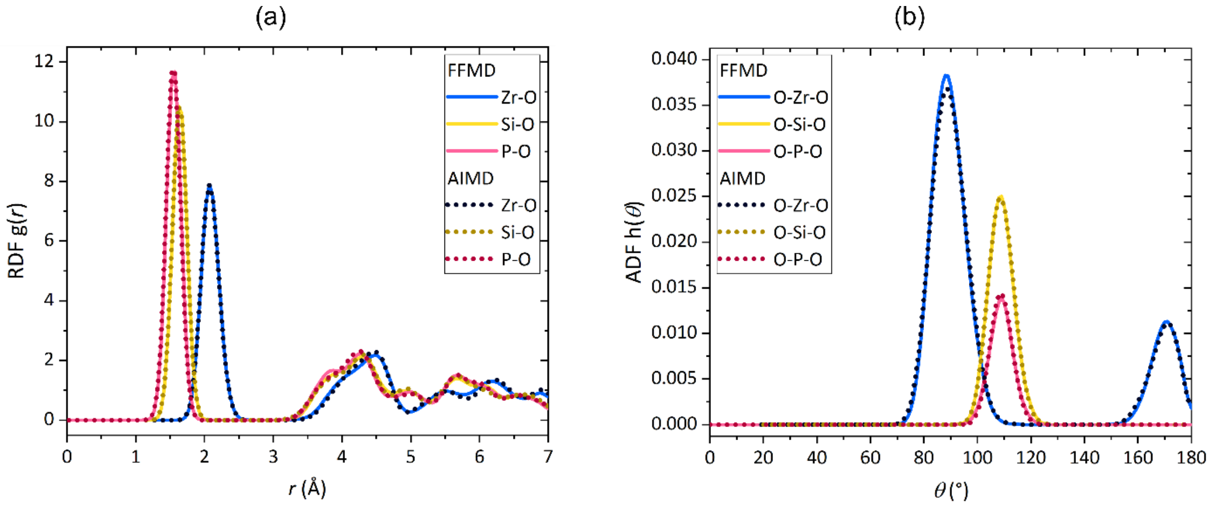

Figure S6. (a) RDFs of cation-O^{2-} pairs and (b) ADFs of O^{2-}–cation-O^{2-} triplets of the structural framework of $Na_3Zr_2Si_2PO_{12}$. The distribution functions obtained by FFMD with FF parameters derived from the (ii) CS optimization are shown as solid lines and those obtained by AIMD are shown as dashed lines.

Step (iii): The FF parameters are further optimized using the co-substituted $Na_3ScZrSiP_2O_{12}$ training system. The FF parameters, which are pre-optimized in step (ii) for the single-substituted composition $Na_3Zr_2Si_2P_1O_{12}$, are applied as initial guess. Fig. S7a displays the evolution of the loss function during the optimization. The CS optimization accomplishes convergence within 1300 CS generations ($L = 5.47 \cdot 10^{-3}$). Fig. S7b illustrates the optimization progress using the parameter D_{ScO} and D_{NaO} in colors according to the values of L. The best parameter set is inside the predefined search space since the initial values are derived from the previous optimization processes. Nevertheless, as the optimization progresses, the final search space narrows to encompass the parameter set with lowest value of L. The density plots along D_{ScO} and D_{NaO} confirm that the method automatically updates the search space leading out of a local minimum outside the search space and searching intensely the best parameter set within the search space.

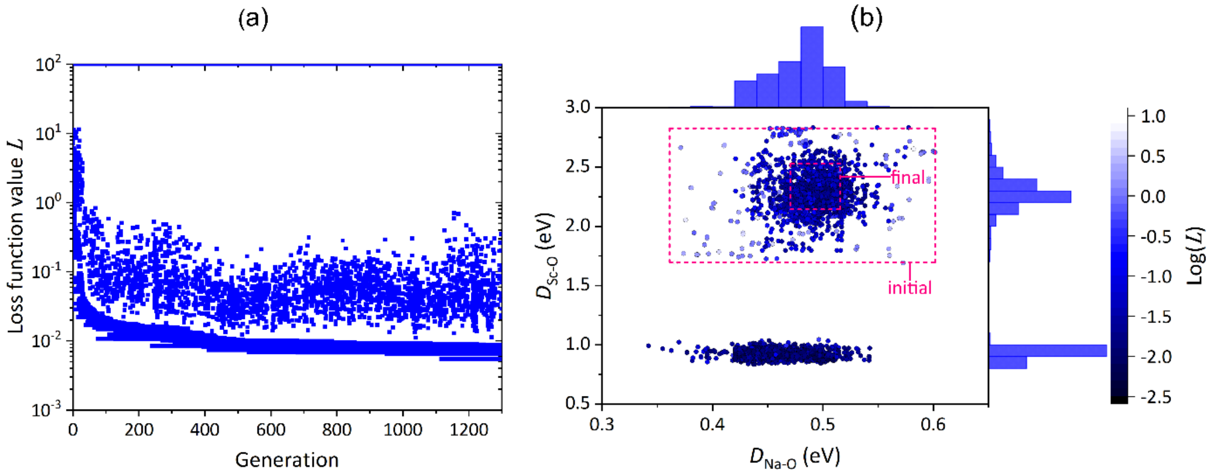

Figure S7. Evaluation of the (iii) CS optimization. (a) Evolution of the loss function L. (b) Values of $D_{\text{Sc-O}}$ and $D_{\text{Na-O}}$ in colors according to L. The initial and final search space are shown in pink dashed lines, the density plots along $D_{\text{Sc-O}}$ and $D_{\text{Na-O}}$ are shown in blue.

Table S3. FF parameters derived from the (iii) CS optimization in the $Na_3ScZrSiP_2O_{12}$ training system. $D_{0,XO}$ is the equilibrium well depth, $r_{0,XO}$ is the equilibrium bond distance between species X and O^{2-}, and α_{XO} is the width of the Morse potential. r_X is the effective ionic radius of species X of the Coulomb potential. λ_{OXO} is the equilibrium well depth and $\gamma_{0,OXO}$ is the equilibrium angle between O^{2-}-X-O^{2-} of the Stillinger Weber potential. X represents the cationic species and O is O^{2-} ions.

Species	$D_{0,XO}$ (eV)	$r_{0,XO}$ (Å)	α_{XO} (Å^{-1})	r_X, r_O (Å)	$\lambda_{0,OXO}$ (eV)	$\gamma_{0,OXO}$ ()
Na^+	0.49	2.18	2.17	1.03	—	—
Sc^{3+}	2.34	1.79	1.89	1.02	0.93	0.25
Zr^{4+}	3.09	1.84	1.65	0.98	1.23	−0.28
Si^{4+}	2.87	1.54	3.10	0.62	1.44	0.29
P^{5+}	5.47	1.43	2.41	0.64	0.89	0.56
O^{2-}	—	—	—	0.89	—	—

The optimized FF parameters listed in Table S3 are employed in FFMD simulations of the $Na_3ScZrSiP_2O_{12}$ training system. The resulting RDFs of cation-O^{2-} pairs and ADFs of O^{2-}-cation-O^{2-} triplets of the structural framework are compared with the results from earlier AIMD simulations. Fig. S8(a, b) illustrates the strong agreement between the RDFs and ADFs derived from both FFMD and AIMD simulations, verifying that the FF parameters accurately reproduce the NaSICON structure.

In addition, the energies and forces acting on the atoms in structures not included in the FF optimization process are compared between AIMD and FF simulations. Therefore, AIMD simulations were performed on Sc- and Si-substituted structure models, specifically $Na_{10}Sc_4Zr_8P_{18}O_{72}$ and $Na_{18}Zr_{12}Si_{12}P_6O_{72}$, at 800 K for 30 ps (30000 steps). From the resulting AIMD trajectory data, 300 structures were extracted. Fig. S8(c)–(f) depicts the diagnostic plots comparing the energy values and forces obtained from AIMD and FFMD simulations, showing good agreement, with an energy difference of up to 3.7 meV per atom and a force difference of up to 0.5 eV Å^{-1}, thereby validating the FF parameters. Although energy values and forces were not explicitly part of the loss function evaluating the optimization process, the strong agreement with the FPMD results at 800 K indicates that the physical model consisting of Coulombic, Morse and SW interactions used in the present FF model reasonably reproduces DFT-derived interactions.

Moreover, Fig. 4 compares the conductivities of $Na_{1+x}Zr_2Si_xP_{3-x}O_{12}$ ($0 \leq x \leq 3$) obtained by the FFMD simulations and reported in literature. The obtained conductivities align well with the literature data, indicating that the FF parameters accurately describe not only the structure but also the interactions between the migrating Na^+ ions and the structural framework as well as the neighboring Na^+ ions.

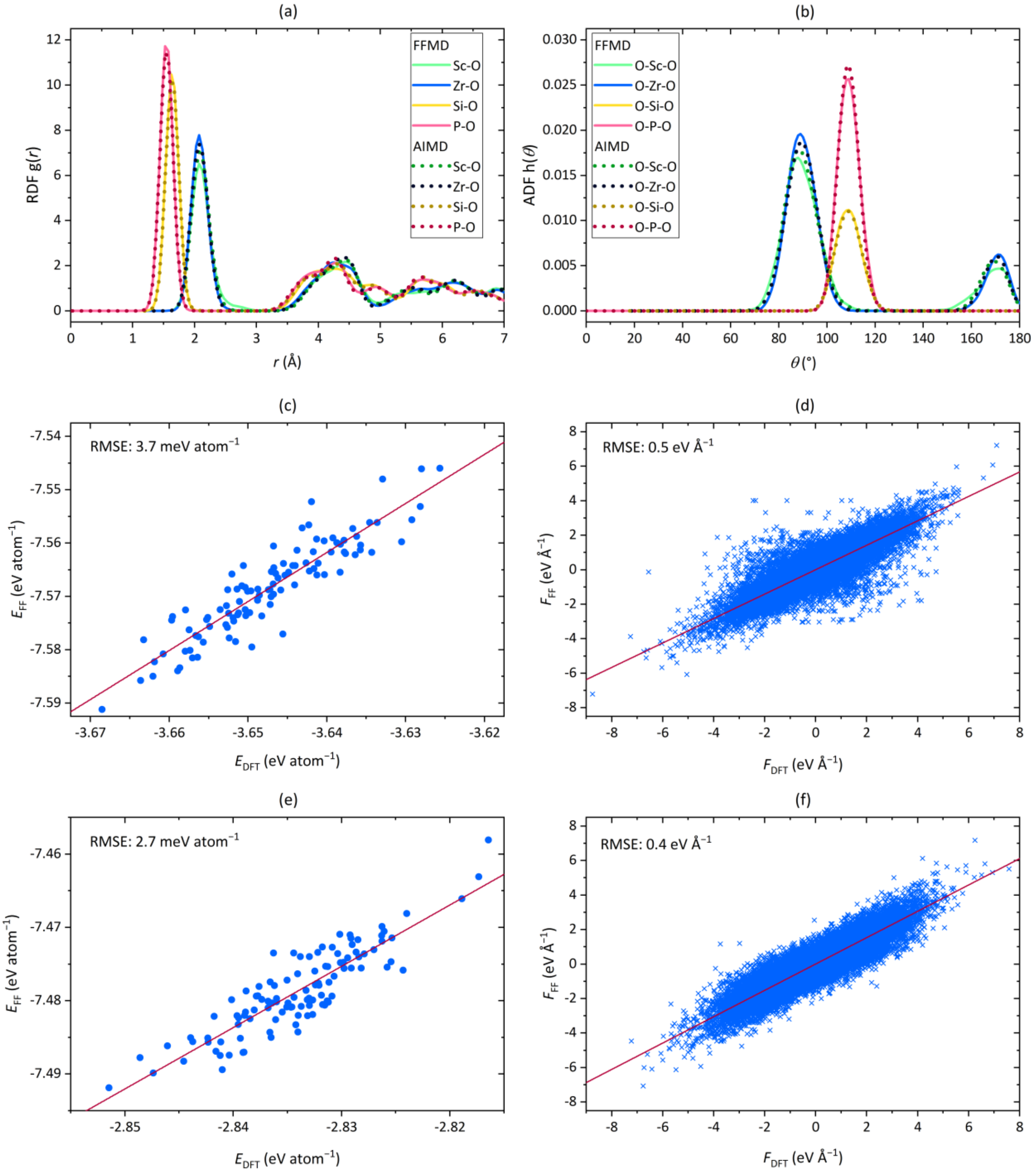

Figure S8. (a) RDFs of cation-O^{2-} pairs and (b) ADFs of O^{2-}-cation-O^{2-} triplets of the structural framework of $Na_3ScZrSiP_2O_{12}$. The distribution functions obtained by FFMD are shown as solid lines and those obtained by AIMD as dashed lines. (c–f) Diagnostic plots of energies and forces acting on atoms in the structures. (c–d) $Na_{10}Sc_4Zr_8P_{18}O_{72}$ and (e–f) $Na_{18}Zr_{12}Si_{12}P_6O_{72}$ comparing the results of AIMD and FFMD simulations.

3. Na^+ Ion Diffusion

The Na^+ diffusion coefficients *D* are determined from the mean squares displacement (MSD) of the Na^+ ions in $Na_{1+x+y}Zr_{2-y}Sc_ySi_xP_{3-x}O_{12}$. Fig. S9 depicts the linear temperature dependence of *D* for certain compositions within the temperature range of $298 \leq T/K \leq 798$, consistent with the Arrhenius relation. The activation energies are calculated according to Eq. 11 considering diffusion coefficients obtained at temperatures between $498 \leq T/K \leq 798$. The linear relationship between *D* and temperature indicates that the number of Na^+ jump events during the MD simulations is statistically significant.

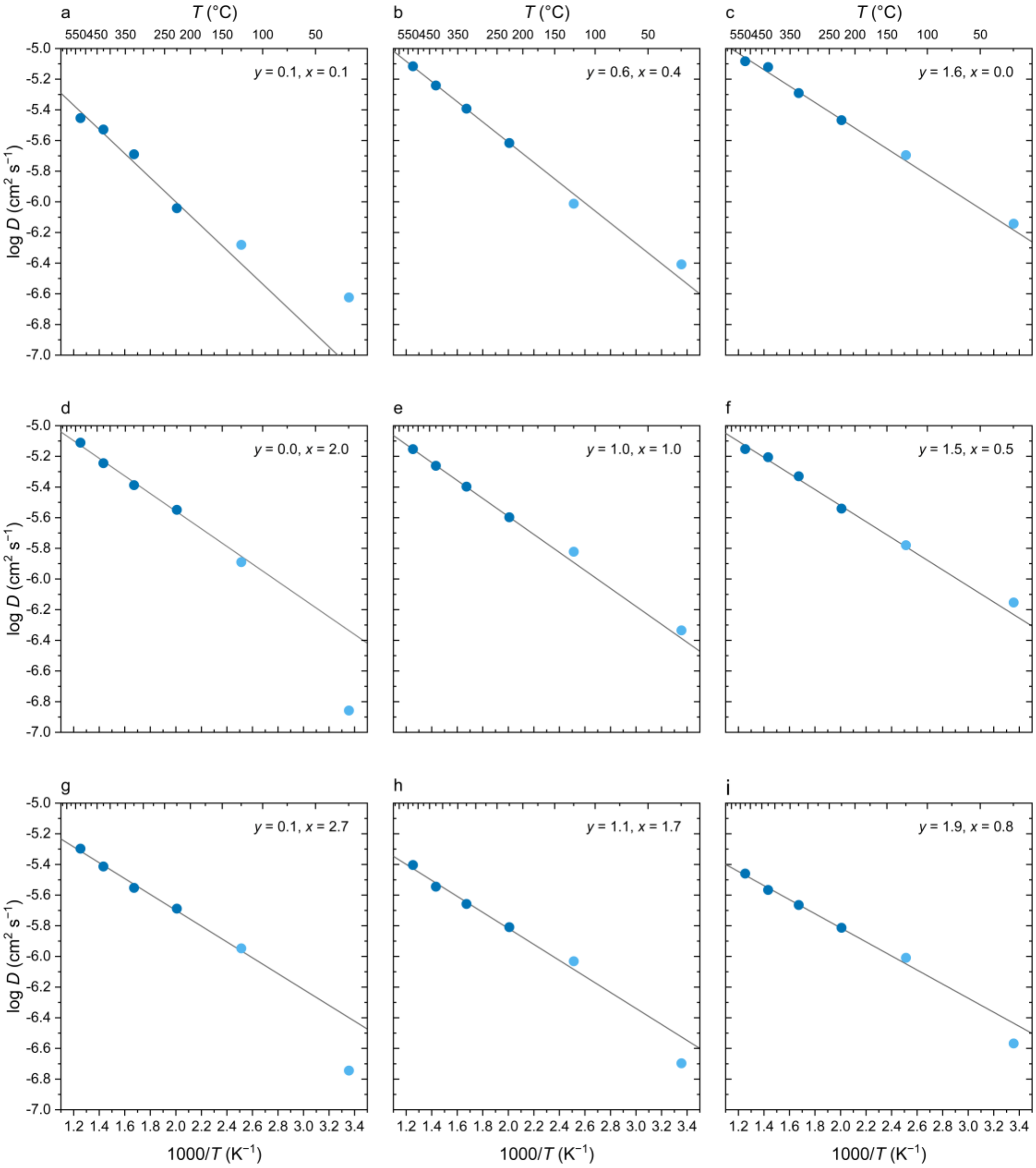

Figure S9. Temperature dependence of diffusion coefficients *D* of $Na_{1+x+y}Sc_yZr_{2-y}Si_xP_{3-x}O_{12}$ with different compositions. The activation energies are calculated according to the Arrhenius relation using the diffusion coefficients obtained at temperatures between $498 \leq T/K \leq 798$ (dark blue) to ensure a statistically significant number of Na^+ jump events, while the diffusion coefficients at 298 K and 398 K (light blue) are neglected.

The impact of different Sc/Zr and Si/P arrangements on the diffusion coefficient of Na was investigated. For 10 randomly selected compositions, four random initial arrangement structures were created, and the relative error in the diffusion coefficient between them was evaluated. The distribution of the obtained diffusion coefficients is shown in Fig. S10. The variation in diffusion coefficients due to differences in arrangement was very small, with the relative standard error being a maximum of 5.6%

and an average of 2.6% across the 10 compositions. Therefore, it was concluded that the supercell size and simulation time (1 ns) applied in this study were sufficiently large.

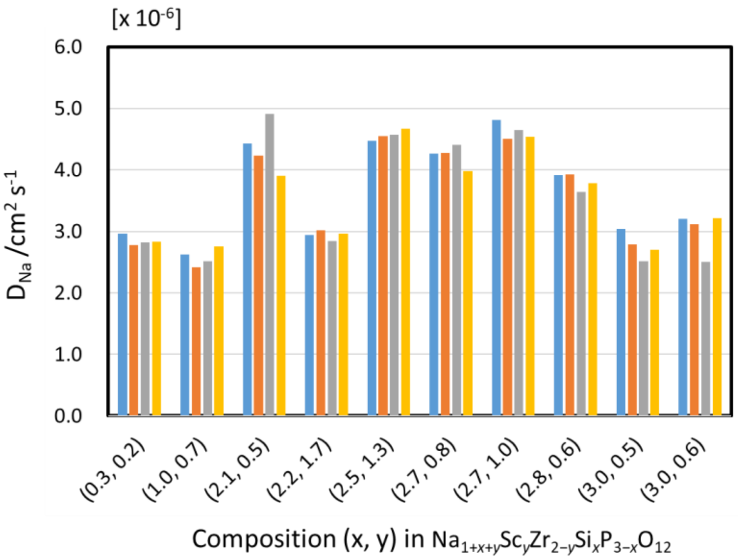

Figure S10. The diffusion coefficients of Na ions calculated through 1 ns MD simulations at 598 K for 10 randomly selected compositions (x, y). For each composition, four random arrangements of Sc/Zr and Si/P were created, and the evaluated diffusion coefficients are shown as blue, orange, gray, and yellow bar graphs.

References

1 J. Rodrigues and A. Zellner, Weighted balanced loss function and estimation of the mean time to failure, *Commun. Stat. Theory Methods*, 1994, **23**, 3609–3616.

2 R. D. Shannon, Revised effective ionic radii and systematic studies of interatomic distances in halides and chalcogenides, *Acta Crystallogr. A.*, 1976, **32**, 751–767.

3 J. B. Goodenough, H.-P. Hong and J. A. Kafalas, Fast Na^+-ion transport in skeleton structures, *Mater. Res. Bull.*, 1976, **11**, 203–220.

4 J. P. Boilot, J. P. Salanie, G. Desplanches and D. Le Potier, Phase transformation in $Na_{1+x}Si_xZr_2P_{3-x}O_{12}$ compounds, *Mater. Res. Bull.*, 1979, **14**, 1469–1477.

5 W. H. Baur, Dygas, JR, D. H. Whitmore and J. Faber, Neutron powder diffraction study and ionic conductivity of $Na_2Zr_2SiP_2O_{12}$ and $Na_3Zr_2Si_2PO_{12}$, *Solid State Ion.*, 1986, **18**, 935–943.

6 D. T. Qui, J. J. Capponi, J. C. Joubert and R. D. Shannon, Crystal structure and ionic conductivity in $Na_4Zr_2Si_3O_{12}$, *J. Solid State Chem.*, 1981, **39**, 219–229.

7 Z. Deng, T. P. Mishra, E. Mahayoni, Q. Ma, A. J. K. Tieu, O. Guillon, J.-N. Chotard, V. Seznec, A. K. Cheetham, C. Masquelier, G. S. Gautam and P. Canepa, Fundamental investigations on the sodium-ion transport properties of mixed polyanion solid-state battery electrolytes, *Nat. Commun.*, 2022, **13**, 4470. DOI: 10.1038/s41467-022-32190-7.

8 J. Schuett, A. S. Kuhn and S. Neitzel-Grieshammer, Predicting the Na^+ ion transport properties of NaSICON materials using density functional theory and Kinetic Monte Carlo, *J. Mater. Chem.*, 2023.

9 J. Schuett, F. Pescher and S. Neitzel-Grieshammer, The origin of high Na^+ ion conductivity in $Na_{1+x}Zr_2Si_xP_{3-x}O_{12}$ NASICON materials, *PCCP*, 2022, **24**, 22154–22167. DOI: 10.1039/D2CP03621E.